SCIENTIFIC REPORTS

OPEN

Selective doping of Ni^{2+} in highly transparent glass-ceramics containing nano-spinels $ZnGa_2O_4$ and $Zn_{1+x}Ga_{2-2x}Ge_xO_4$ for broadband near-infrared fiber amplifiers

Received: 19 October 2016
Accepted: 31 March 2017
Published online: 11 May 2017

Zhigang Gao[1], Yinyao Liu[2], Jing Ren[1,3], Zaijin Fang[1], Xiaosong Lu[1], Elfed Lewis[4], Gerald Farrell[5], Jun Yang[1] & Pengfei Wang[1,5]

Selective doping of Ni^{2+} in octahedral sites provided by nanocrystals embedded in glass-ceramics (GCs) is crucial to the enhancement of broadband near-infrared (NIR) emission. In this work, a NIR emission with a full-width-at-half-maximum (FWHM) of 288 nm is first reported from $ZnGa_2O_4$: Ni^{2+} nano-spinels embedded GCs with excellent transparency. A comparison is made of the NIR luminescence properties of Ni^{2+} doped GCs containing $ZnGa_2O_4$, germanium-substituted $ZnGa_2O_4$ nano-spinels ($Zn_{1+x}Ga_{2-2x}Ge_xO_4$), and $Zn_2GeO_4/Li_2Ge_4O_9$ composite nanocrystals that are free of Ga^{3+}. The results show that $ZnGa_2O_4$: Ni^{2+} GCs exhibit a significantly enhanced NIR emission. The incorporation of the nucleating agent TiO_2 is favored in terms of the increased luminescence intensity and prolonged lifetime. The possible causes for the enhancement effect are identified from the crystal structure/defects viewpoint. The newly developed GCs incorporate good reproducibility to allow for a tolerance of thermal treatment temperature and hence hold great potential of fiberization via the recently proposed "melt-in-tube" method. They can be considered as promising candidates for broadband fiber amplifiers.

Broadband tunable near-infrared (NIR) light sources are extremely useful for a wide range of applications in optical communications, photochemistry, spectroscopy and pump-probe experiments etc.[1]. The ability of transition metal (TM) ions (e.g., Ti^{3+}, V^{3+}, Cr^{3+}, Cr^{4+}, Ni^{2+} etc.) doped bulk crystals and glass-ceramics (GCs) to lase in the broadly tunable NIR (1000~1700 nm) wavelength region have attracted intense attention over the last two decades[2–6]. Because nickel is very stable in its divalent oxidation state (Ni^{2+}), Ni^{2+} doped phosphors can be readily synthesized in ordinary lab conditions without strict valence control[7]. However, Ni^{2+} cannot lase in glasses because Ni^{2+} is generally five-fold (trigonal bipyramidally, $^5Ni^{2+}$) and/or four-fold (tetrahedrally, $^4Ni^{2+}$) coordinated in glassy networks[8], whereas only six-fold octahedrally coordinated $^6Ni^{2+}$ exhibits luminescence in the NIR wavelength range. Even when Ni^{2+} adopts an octahedral coordination in fluoride glasses[9], the strong electron-phonon coupling of $^6Ni^{2+}$ in amorphous materials severely limits the radiative quantum efficiency. These problems can be resolved provided GCs containing nanocrystals that provide octahedral sites for Ni^{2+} can be produced, which is very possible through ingenious composition design and well controlled crystallization[10]. Selective doping of $^6Ni^{2+}$ in $ZnAl_2O_4$[11], $LiGa_5O_8$[12–14], Ga_2O_3[15] and most recently ZnF_2 and $KZnF_3$[2,17] embedded

[1]Key Lab of In-fiber Integrated Optics, Ministry Education of China, Harbin Engineering University, Harbin, 150001, China. [2]Key Lab of Materials for High Power Laser, Shanghai Institute of Optics and Fine Mechanics, CAS, Shanghai, 201800, China. [3]Jiangsu Key Laboratory of Advanced Laser Materials and Devices, School of Physics and Electronic Engineering, Jiangsu Normal University, Xuzhou, Jiangsu, China. [4]Optical Fibre Sensors Research Centre, Department of Electronic and Computer Engineering, University of Limerick, Limerick, Ireland. [5]Photonic Research Centre, Dublin Institute of Technology, Kevin Street, Dublin 8, Ireland. Correspondence and requests for materials should be addressed to J.R. (email: ren.jing@hrbeu.edu.cn) or P.W. (email: pwang@hrbeu.edu.cn)

transparent GCs and even glass-ceramic (GC) optical fibers have been produced[16]. Promising results such as the ligand-field driven wavelength tunable and broadband NIR emission of Ni^{2+} have also been observed[5,17].

The pursuit of Ni^{2+} doped GCs is being driven continuously by newly invented crystals with excellent luminescence properties, for example, the germanium-substituted $ZnGa_2O_4$ spinel of the general formula $Zn_{1+x}Ga_{2-2x}Ge_xO_4$ ($0 \leq x \leq 1$) and this has attracted significant attention due to the unprecedented persistent luminescence observed in $Zn_{1+x}Ga_{2-2x}Ge_xO_4$:Cr^{3+} [18]. Such nanocrystals can simultaneously provide tetrahedral (occupied by $^4Zn^{2+}$ and $^4Ge^{4+}$) and octahedral (occupied by $^6Ga^{3+}$) sites for Mn^{2+}, Co^{2+}, Ni^{2+}, Cr^{3+} and Mn^{4+} etc., and thus can be used as a multi-functional platform for diverse applications in lighting, display, telecommunication and bio-imaging etc.[19–21]. Additionally, transparent GCs containing $Zn_{1+x}Ga_{2-2x}Ge_xO_4$ nanocrystals have been recently fabricated[21,22]. Selective doping of Ni^{2+} in $Zn_{1+x}Ga_{2-2x}Ge_xO_4$ nanocrystals embedded in GCs has been reported; however, the NIR luminescence properties were not clearly identified in this case[22]. To date the authors of this article are not aware of any study relating to the luminescence properties of $ZnGa_2O_4$: Ni^{2+} GCs, although GCs containing $ZnGa_2O_4$: Cr^{3+} nanocrystals, showing persistent luminescence and temperature sensing properties, have recently been extensively studied[12,23].

In the work reported in this article a detailed study has been undertaken and comparison made of the NIR luminescence properties of Ni^{2+} doped GCs containing $ZnGa_2O_4$ and germanium-substituted $ZnGa_2O_4$ ($Zn_{1+x}Ga_{2-2x}Ge_xO_4$) nano-spinels. To underline the important role of $^6Ga^{3+}$, other Ni^{2+} doped GCs containing $Zn_2GeO_4/Li_2Ge_4O_9$ composite nanocrystals that are free of Ga^{3+} were also prepared for comparison. The synthesized $ZnGa_2O_4$: Ni^{2+} GCs are highly reproducible which allows for a tolerance of thermal treatment temperature, and thus are perfectly matched for the recently proposed "melt-in-tube" method. For functional GC fibers cannot be obtained using the conventional "rod-in-tube" method[16,24–26], the 'melt-in-tube method has recently facilitated fabrication of GC fibers doped with Ni^{2+} [16], Bi[24], Cr^{3+} [25], or quantum dots[26] which have exhibited excellent optical quality. The study described in this article is expected not only provide a candidate fiber amplifier material, but also advance understanding of the correlation between the structure of the nanocrystals and NIR luminescence of Ni^{2+}, and thus will provide useful guidance for designing novel Ni^{2+} doped GCs with enhanced luminescence properties such as ultra-broadband tunable NIR emission[27]. Moreover, the present work may also advance the understanding of the mechanism underlying the persistence luminescence of Cr^{3+} doped spinels which is currently still open to question[18].

Experiments

Three different types of the nominal composition (in mol. %) of Ni^{2+}-doped glasses and GCs were prepared using high purity (4N) raw materials of SiO_2, GeO_2, Ga_2O_3, ZnO, Na_2CO_3, K_2CO_3, Li_2O, ZrO_2, TiO_2 and NiO.

1) **$51SiO_2$-$18Ga_2O_3$-18ZnO-$6Na_2O$-$4ZrO_2$-$3TiO_2$-*x*NiO** ($x = 0$, 0.15, 0.3, 0.5) was chosen to generate the $ZnGa_2O_4$ nanocrystal, hereafter, this group of glasses and glass-ceramics are denoted as ZGO-*x*PG and ZGO-*x*GC, respectively. Glasses were melted in a platinum crucible at 1600 °C for 2 h, quenched onto a cold brass plate and then annealed at 500 °C for 3 h. GCs were fabricated by heating the annealed glasses at 680 °C for 12 h followed by a further heating at 780~800 °C for 12 h, refer to Tanaka *et al.*[28];
2) **$62GeO_2$-20ZnO-$10Ga_2O_3$-$5K_2CO_3$-$3TiO_2$-*x*NiO** ($x = 0$, 0.15, 0.3 and 0.5) was chosen to generate $Zn_{1+x}Ga_{2-2x}Ge_xO_4$ nanocrystal, hereafter, this group of glasses and glass-ceramics are denoted as ZGGO-*x*PG and ZGGO-*x*GC, respectively. Glasses were preheated at 850 °C for 30 min and then melted in an alumina crucible at 1400 °C for 30 min. The glasses were then annealed at 500 °C for 3 h. GC was made via a heat-treatment at 650 °C for 2 h, as described in ref. 21;
3) **$70GeO_2$-15ZnO-$15Li_2O$-0.15NiO** was chosen to generate Zn_2GeO_4 and $Li_2Ge_4O_9$ nanocrystal, hereafter, this group of glasses and glass-ceramics are denoted as ZLGO-0.15PG and ZLGO-0.15GC, respectively. The glasses were melted in a platinum crucible at 1300 °C for 30 min and annealed at 450 °C for 2 h. GCs were fabricated by heating the annealed glasses at 545 °C for 2 h, similar to the process reported in ref. 29.

Transmission spectra were measured using a Perkin-Elmer Lambda 950 UV-VIS spectrophotometer in the spectral range of 200–1800 nm. Refractive indices were measured using an Abbe refractometer AR2008 (KRÜSS, Germany). Photoluminescence (PL) spectra were recorded using a Fluorolog-3-P UV-vis-NIR fluorescence spectrophotometer (JobinYvon, Longjumeau, French). The decay curves were measured using a FLS920 Fluorescence spectrometer (Edinburgh Instruments) from room temperature (300 K) down to liquid helium temperature (10 K). The samples used for the PL measurement were plane-parallel well polished plates with the identical dimension of ~$10 \times 10\,mm^2$ and thickness of 1 mm. The fluorescence was collected in the direction perpendicular to the direction of the pump beam, and the pump light was focused (to a spot of diameter ~4 mm) using a lens and incident at a 45° angle to the normal of the front surface of the sample. In the experiment, both the power of the pump light and the configuration of the light path were kept the same. Because only very thin samples were used for the measurement, reabsorption is not significant and any effects due to this can be omitted in the present study, in accordance with the work of Loiko[30].

X-ray diffraction (XRD) patterns of all the samples were recorded under the same measurement conditions using an X-ray diffractometer (D/MAX 2550VB/PC, Rigaku Corproation, Japan) with Cu-Kα irradiation. The microstructure of the crystallized glasses was studied using a JEM-2100 high-resolution transmission electron microscope (HRTEM). Raman spectra were measured by RenishawInvia Raman microscope (Renishaw, Gloucestershire, UK) with an excitation wavelength of 515 nm.

Results and Discussion

From the XRD patterns of the crystallized glasses, the precipitation of $ZnGa_2O_4$ (Fig. 1(a)), and $Zn_{1+x}Ga_{2-2x}Ge_xO_4$ nano-spinels (Fig. S1(a), supporting information), as well as $Zn_2GeO_4/Li_2Ge_4O_9$ composite phases (Fig. S2 in the

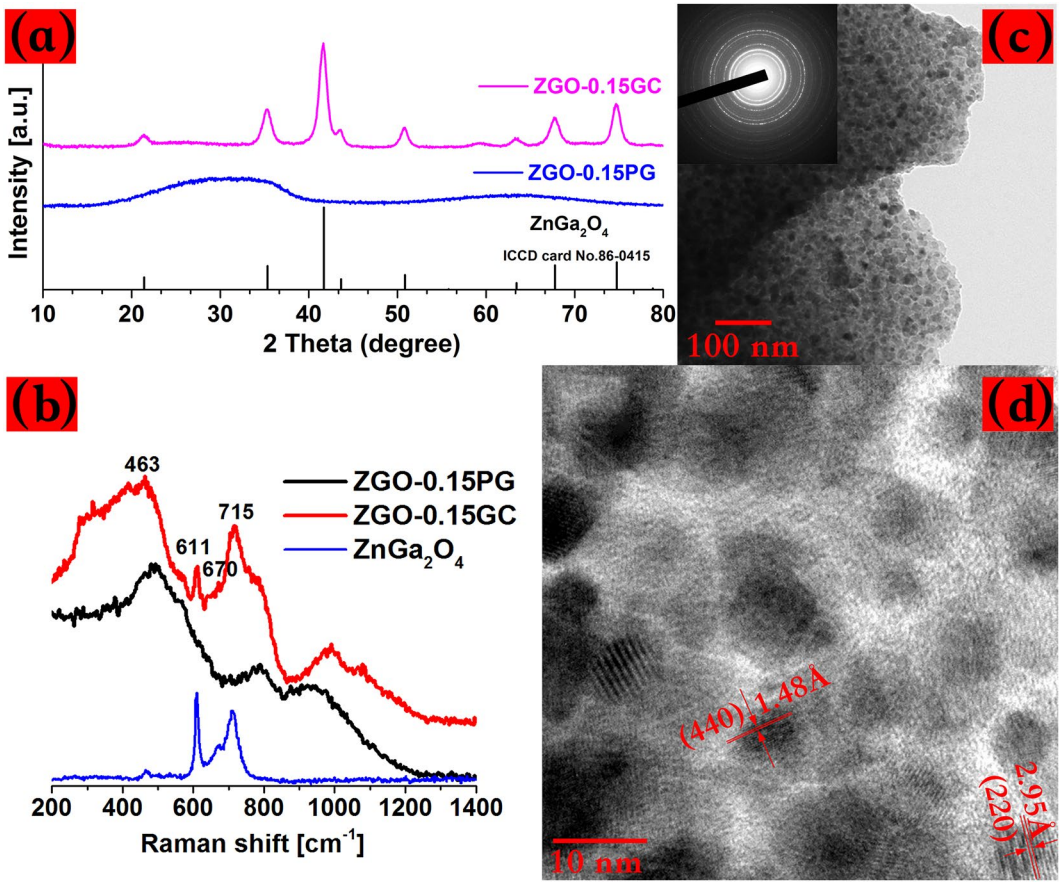

Figure 1. (**a**) XRD patterns of the as-made Ni^{2+} doped glass (ZGO-0.15PG), crystallized glass (ZGO-0.15GC) and standard $ZnGa_2O_4$ crystal (PDF card no. 86–0415); (**b**) Raman spectra of the as-made glass (ZGO-0.15PG), crystallized glass (ZGO-0.15GC) and standard $ZnGa_2O_4$ polycrystals; (**c**) TEM bright-field image of the crystallized glass; (**d**) HRTEM image of the selected area. Inset in (**c**): Selected-area electron diffraction (SAED) pattern.

supporting information) can be discerned in accordance to the literature[21,28,29]. The formation of the target nanocrystals were also confirmed from the Raman spectra where the crystallized glasses show sharp scattering peaks well match those of the standard polycrystals (Fig. 1(b)). According to the work of Zhuang *et al.*[21], it is very difficult to determine unambiguously the exact $Zn_{1+x}Ga_{2-2x}Ge_xO_4$ phase in GCs, owing to the undistinguishable XRD patterns between the two end-members, $ZnGa_2O_4$ ($x=0$) and Zn_2GeO_4 ($x=1$). By comparing the Raman spectra of the crystallized glasses with the standard $Zn_{1+x}Ga_{2-2x}Ge_xO_4$ polycrystals synthesized in our lab by solid-state reaction (for more detail, refer to our previous work[19]), we provide the first direct evidence for the formation of $Zn_{1+x}Ga_{2-2x}Ge_xO_4$ with $x \geq 0.4$ in GCs (Fig. S1(b), supporting information).

The crystallinity (volume fraction of the crystalline phase) of the GCs can be estimated by the ratio of the area under the indexed diffraction peaks to that under the whole XRD patterns[14]. For $ZnGa_2O_4$ and $Zn_{1+x}Ga_{2-2x}Ge_xO_4$ GCs, the crystallinities are approximately 37% and 32%, respectively, which are close in value to each other. The total molar concentration of ZnO and Ga_2O_3 is only 36 mol. % for the $ZnGa_2O_4$ GCs, which is less than the calculated crystallinity. The reason for the discrepancy is not clear and the validity of this result has yet to be confirmed. Here, it should be noted that the presence of nucleating agent such as TiO_2 in gallium-containing GCs favors the substitution of $^6Ni^{2+}$ (ionic radius: 0.69 Å) for $^6Ga^{3+}$ (ionic radius: 0.62 Å) via the following substitutional mechanism: $Ti^{4+} + Ni^{2+} \rightarrow 2Ga^{3+}$, where Ti^{4+} acts as charge compensator[31,32]. The incorporation of Ti^{4+} in the precipitated nanospinels was confirmed by the TEM-EDS analysis on the selected crystallization area in the ZGO-0.15GC sample (Fig. S3, supporting information). It is possible that a certain degree of inversion may occur in realistic spinels during crystallization, i.e., a fraction of the Ni^{2+} can occupy non-luminescent tetrahedral sites as found in $NiAl_2O_3$ crystals[33,34], and hence the selective doping of Ni^{2+} in octahedral sites is highly desirable for enhanced NIR luminescence[33].

The morphology, distribution and particle sizes of nanocrystals were determined from the HRTEM measurements. The precipitated nanoparticles, approximately 15 nm in diameter, are distributed uniformly in all the GCs (Fig. 1(c) and (d)). The ultra-fine particle size allows these materials to be polished as they are in the glass state and then crystallized without any significant degradation of the surface quality (shown photographically in Fig. 2(a) and Figs S4 and S5, supporting information). The crystallization process was highly reproducible as

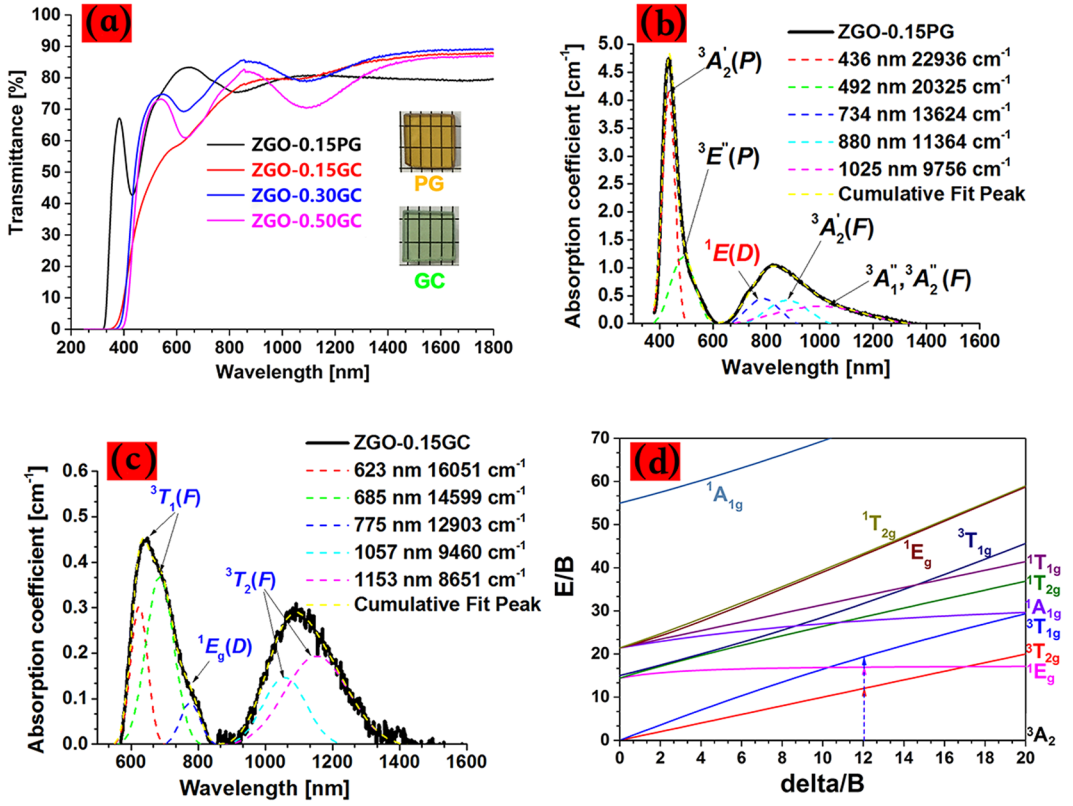

Figure 2. (**a**) Transmission spectra of the ZGO glasses and GCs of varying NiO; Absorption spectra of the ZGO-0.15PG glass (**b**) and ZGO-0.15GC glass ceramic (**c**) obtained after subtracting the background absorption. The absorption bands can be well fitted by Gauss function, and those related to ^{6}Ni, ^{5}Ni, ^{4}Ni are indicated by blue, black and red colors, respectively; (**d**) Tanabe-Sugano (TS) diagram for the octehedrally coordinated Ni^{2+} investigated in the work.

verified by the fact that GCs show similar performance can be obtained repeatedly under the same experimental condition.

The coordination states of Ni^{2+} can be approximately inferred from the color of the glasses and GCs, for example, blue, brown and yellow-green in the case of $^{4}Ni^{2+}$, $^{5}Ni^{2+}$, and $^{6}Ni^{2+}$ coordination, respectively[8]. The as-made ZGO (Fig. 2(a)) and ZGGO glasses (Fig. S4, supporting information) are light brown in appearance, suggesting $^{5}Ni^{2+}$ and $^{4}Ni^{2+}$ coordination states, whereas the color of the crystallized glasses becomes light green and blue, indicative of $^{6}Ni^{2+}$. Since $^{6}Ni^{2+}$ possesses a larger crystal field stabilization energy (CFSE) value than that of $^{5}Ni^{2+}$, the unstable $^{5}Ni^{2+}$ in glasses tends to transform into $^{6}Ni^{2+}$ during crystallization of the spinel phases. The absorption related to $^{6}Ni^{2+}$ (e.g., around 1160 nm due to the $^{3}A_2(^{3}F) \rightarrow {}^{3}T_2(^{3}F)$ transition) in GCs increases with the concentration of NiO, indicative of an efficient partition of Ni^{2+} in $ZnGa_2O_4$ nanocrystals, e.g. more than 90% of Ni^{2+} can be successfully embedded in gallium-containing GCs[7], whereas it is well known that substitutional doping a large fraction of TM ions into semiconductor nanocrystals is extremely difficult because of the intrinsic self-purification mechanism[35]. The absorption bands can be well fitted to the Tanabe-Sugano (TS) diagram for d^8 ions (Fig. 2(d)), with the values of Racah parameter (B) and crystal field strength (Dq) equal to 767 cm^{-1} and 917 cm^{-1}, respectively.

An inspection of the transmission spectra of the $Zn_2GeO_4/Li_2Ge_4O_9$ GCs (Fig. S5, supporting information) also indicates the presence of $^{6}Ni^{2+}$, which is possible via the substitution of $^{6}Ni^{2+}$ for $^{6}Ge^{4+}$ in $Li_2Ge_4O_9$ nanocrystals. Meanwhile, since both the valence and ionic radius of $^{4}Zn^{2+}$ (0.60 Å) matches those of $^{4}Ni^{2+}$ (ionic radius: 0.55 Å), the substitution of $^{4}Ni^{2+}$ for $^{4}Zn^{2+}$ in $ZnGa_2O_4$ and Zn_2GeO_4 nanocrystals may also occur, similar to the embedding of Ni^{2+} in Zn_2SiO_4 crystals[36]. For a detailed analysis and discussion of the absorption spectra, refer to Supporting Information (Fig. S6). The fabricated GCs with transmission larger than 80% demonstrate great potential to be drawn into fibers for use as fiber lasers and amplifiers.

The use of the nucleant TiO_2 is very important; it drastically increases both the emission intensity (Fig. S7, supporting information) and lifetime (Fig. S8, supporting information) of the GCs as compared to those free of TiO_2 but otherwise the GCs containing TiO_2 were thermally treated under identical conditions. The enhancement effect can be understood based on the substitution mechanism by which Ni^{2+} substitutes for Ga^{3+} favorably as mentioned above. An intense broadband NIR emission (from 1100 to 1700 nm) was recorded from $ZnGa_2O_4$: Ni^{2+} and $Zn_{1+x}Ga_{2-2x}Ge_xO_4$: Ni^{2+} GCs, but was very weak from $Zn_2GeO_4/Li_2Ge_4O_9$: Ni^{2+} GCs. Both the emission intensity (Fig. 3(a)) and lifetime (Fig. 3(b)) (defined as the time taken for the emission intensity to decay to $1/e$ of its initial value) increase with NiO for the $Zn_{1+x}Ga_{2-2x}Ge_xO_4$: Ni^{2+} GCs, in contrast to $ZnGa_2O_4$: Ni^{2+} GCs

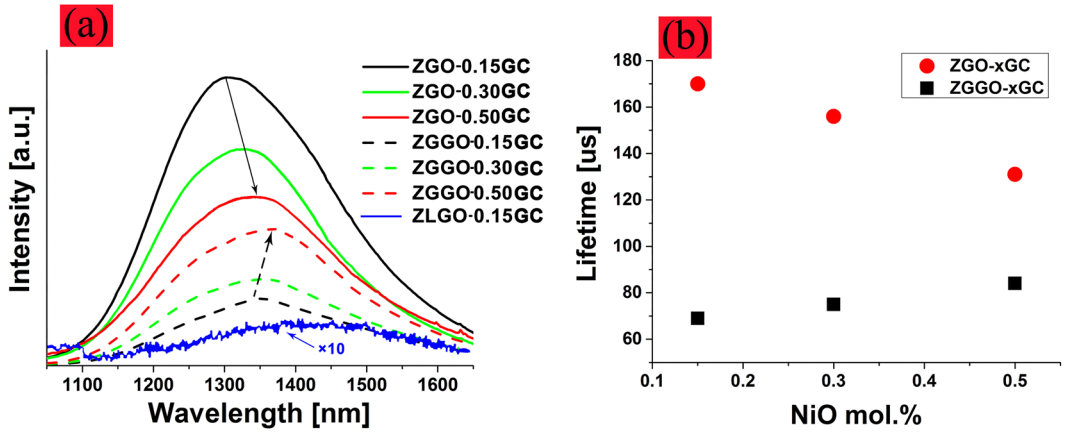

Figure 3. (**a**) Emission spectra of $ZnGa_2O_4$: Ni^{2+} (ZGO-*x*GC, solid lines) and $Zn_{1+x}Ga_{2-2x}Ge_xO_4$: Ni^{2+} (ZGGO-*x*GC, dashed lines) nanocrystals embedded GCs with varying NiO (*x*, mol. %). Also shown is that of Zn_2GeO_4/$Li_2Ge_4O_9$: Ni^{2+} embedded GCs (ZLGO-0.15GC, dotted line) with the intensity multiplied by an order of ten for the purpose of clarity; (**b**) Lifetime of the NIR emission of the ZGO and ZGGO GCs as a function of NiO.

where concentration quenching has already set in at the lowest doping level (~0.15 mol. %). However, in the cases with a fixed NiO, the $ZnGa_2O_4$: Ni^{2+} GCs exhibit stronger NIR emission and longer lifetime than those of $Zn_{1+x}Ga_{2-2x}Ge_xO_4$: Ni^{2+} GCs, e.g., a five-fold increase in the intensity and a two-fold increase in the lifetime when NiO was 0.15 mol. %. For the $Zn_{1+x}Ga_{2-2x}Ge_xO_4$: Ni^{2+} GCs, the emission intensity appears not to saturate at 0.5 mol. %. GCs have also been fabricated doped with 0.7 mol. % NiO. However, the samples suffer from significant devitrification due to NiO-assisted growth of large sized crystals commonly found in glasses heavily doped with NiO[7]. As a result, the 0.7 mol. % doped GCs become opaque and this restricts their use for optical applications, and hence does not warrant further study.

The differences in the crystal structures between the ZGO and ZGGO GCs may account for the contrast in the luminescent property. The $Zn_{1+x}Ga_{2-2x}Ge_xO_4$ crystals were assumed to be a solid solution between the normal $ZnGa_2O_4$ and inverted Zn_2GeO_4 spinel structures[19,37]. Pure $Zn_{1+x}Ga_{2-2x}Ge_xO_4$ spinels can be synthesized for *x* ranging from 0 to 0.5[19]. Our recent study of Mn doped $Zn_{1+x}Ga_{2-2x}Ge_xO_4$ phosphors shows that the substitution of Ge^{4+} for octahedrally coordinated $^6Ga^{3+}$ helps to separate Mn^{4+} which also substitutes for $^6Ga^{3+}$, thus resulting in an enhanced emission of Mn^{4+}[38]. It is assumed that a similar separating effect exists for Ni^{2+} as well, i.e., $^6Ni^{2+}$ ions are well separated in the ZGGO GCs, and thus the concentration quenching is postponed. As more Ni^{2+} ions diffuse from the surface to the inside of the nanocrystals and/or are shielded by the nanocrystals from the outside high-phonon energy environment, the non-radiative relaxation rate is reduced, and the lifetime increases accordingly. However, in the case of $ZnGa_2O_4$ GCs, Ni^{2+} substituting for $^6Ga^{3+}$ is not well separated because there is no "separating agent" akin to Ni^{2+} doped Ga_2O_3 GCs where concentration quenching already starts at 0.10 mol. % low content of Ni^{2+}[7], and this accounts for the observed decreasing lifetime in the ZGO GCs.

Previous studies have shown that the Cr^{3+}-doped and germanium-substituted compounds ($Zn_{1+x}Ga_{2-2x}Ge_xO_4$, $x \leq 0.5$) exhibit much brighter and longer persistence luminescence than pure Cr^{3+}-doped $ZnGa_2O_4$ spinels[37]. The $2Ga^{3+} \rightarrow Ge^{4+} + Zn^{2+}$ substitution induces an inversion increase in the spinel structure, that is, an increased amount of Ga^{3+} now occupies the tetrahedral $^4Zn^{2+}$ sites, forming the so-called anti-site defects ($Ga_{Zn}^{\bullet}$). According to ref. 37, the enhancement of Cr^{3+} emission relies on the formation of anti-site defects, however, the presence of such defects definitely has an adverse effect on the luminescence of Ni^{2+} because of the reduced proportion of $^6Ga^{3+}$ sites. On the other hand, it is possible that the substitution of Ge^{4+} for $^6Ga^{3+}$ may generate octahedrally coordinated $^6Ge^{4+}$, which may in turn be substituted by Ni^{2+}. However, considering the fact that only weak NIR emission was observed from the Zn_2GeO_4/$Li_2Ge_4O_9$: Ni^{2+} GCs, and the large mismatch in valence and ionic radii between $^6Ni^{2+}$ and $^6Ge^{4+}$ (ionic radius: 0.53 Å), the substitution of $^6Ni^{2+}$ for $^6Ge^{4+}$ is severely limited, akin to the partition of Ni^{2+} in K_2SiF_6 nanocrystals embedded GCs[17]. Moreover, no NIR emission related to the tetrahedrally coordinated $^4Ni^{2+}$, e.g., Ni^{2+} doped Zn_2SiO_4 or Zn_2GeO_4 crystals, has been recorded even at cryogenic temperatures[36]. All these effects account for the observed weaker emission intensity of the ZGGO GCs than that of the ZGO GCs.

The $ZnGa_2O_4$: Ni^{2+} GCs, were selected for further study of internal fluorescence quantum efficiency (η) due to the stronger NIR emission and longer lifetime of Ni^{2+}. Figure 4 shows the NIR emission lifetime of Ni^{2+} as a function of temperature from room temperature (300 K) down to liquid helium temperature (10 K). The sudden drop in lifetime at around 100 K indicates the occurrence of phonon-assisted non-radiative relaxation[39]. As shown in the inset, the decay curve has a strong non-exponential characteristic, implying multiple site effects of Ni^{2+} and non-radiative multipolar interactions among Ni^{2+}. The value of η can be calculated as $\eta = \tau_{300K}/\tau_{0K}$, where τ_{300K} (~0.17 ms) and τ_{0K} (~0.62 ms, obtained by linear extrapolation to 0 K) are the lifetimes at the room and absolute zero temperatures, respectively. It is about 25% for the $ZnGa_2O_4$: Ni^{2+} GCs, which is less than that of $ZnAl_2O_4$: Ni^{2+} (~55%)[40], $LiGa_5O_8$: Ni^{2+}(~60%)[12] and $BaAl_2Ti_6O_{16}$: Ni^{2+} (~65%)[39] GCs. However, it is comparable to that of Ga_2S_3: Cr^{4+} chalcogenide GCs (~25%)[4] and even larger than that of pure Ni^{2+} doped $ZnGa_2O_4$ crystals (~18%)[41].

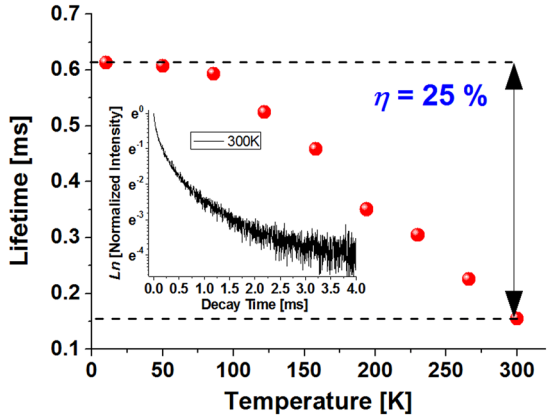

Figure 4. Temperature dependence of the NIR emission lifetime of Ni^{2+} doped ZGO GCs. Inset: the decay curve of the NIR emission of Ni^{2+} at the room temperature, those measured at other temperatures have a similar profile and thus are not shown.

	$ZnGa_2O_4$	$Zn_{1+x}Ga_{2-2x}Ge_xO_4$	$(Ga_2O_3)_3(GeO_2)_2$	$LiGa_5O_8$	β-Ga_2O_3	$ZnAl_2O_4$	Pr^{3+}	Dy^{3+}
$^3T_{2g}(^3F)$ (cm^{-1})	9174	9091	9708	9483	9891	9066		
$^1E_g(^1D)$ (cm^{-1})	12903	12903	13737	12987	13158	14124		
$^3T_{1g}(^3F)$ (cm^{-1})	15504	15149	16189	15949	16502	14517		
Dq (cm^{-1})	917	909	971	948	989	907		
B (cm^{-1})	767	712	887	895	892	940		
λ_{peak} (nm)	1320	1350	1300	1300	1200	1350	1344	1340
τ_{298K} (μs)	170†/525‡	70†/258‡	254‡	583‡	665‡	240‡	360†	38†
FOM $\times 10^{-24}$ cm^2·s	1.23†/3.8‡	/	/	3.7‡	/	3.1‡	4.79†	1.4†
Ref.	this work	this work	5	12	45	31, 40	42	43–44

Table 1. Comparison of luminescent properties and crystal field parameters of GCs containing different nanospinels. Rare earth (Pr^{3+} or Dy^{3+}) doped glasses emitting at similar *O*-band wavelengths are also listed for comparison. †1/*e* lifetime and ‡average lifetime.

The stimulated emission cross section (σ_e) was calculated using the McCumber formula[4] and was found to be 0.52×10^{-20} cm^2. The product of σ_e and τ_{300K} (proportional to the amplification gain and inversely proportional to the laser oscillation threshold) taken as a figure of merit (FOM) for the ZGO-0.15GC sample is 1.23×10^{-24} cm^2·s if the 1/*e* lifetime is used for the calculation, and is about 3.79×10^{-24} cm^2·s if the average lifetime $\tau_m = \int tI(t)dt / \int I(t)dt$ is used for the calculation, which is comparable to that of $ZnAl_2O_4$: Ni^{2+} (~3.1×10^{-24} cm^2·s)[40], $LiGa_5O_8$: Ni^{2+} (~3.7×10^{-24} cm^2·s)[12] and $BaAl_2Ti_6O_{16}$: Ni^{2+} (~3.3×10^{-24} cm^2·s)[39] GCs, and much larger than Ga_2S_3: Cr^{4+} chalcogenide (ChG) GCs (~0.62×10^{-24} cm^2·s) which are known for the difficulty of preparation[4]. Light amplification at similar *O*-band wavelengths can be also achieved for Pr^{3+} or Dy^{3+} doped fluoride and ChG glasses of very low phonon energy. In comparison, the FOM of the ZGO-0.15GC is less than that of Pr^{3+} doped Ge-Ga-S ChG glass (4.79×10^{-24} cm^2·s)[42], however, it is much larger than in the case of Pr^{3+} doped ZBLAN (0.38×10^{-24} cm^2·s) and Dy^{3+} doped Ge-Ga-S ChG glasses (1.4×10^{-24} cm^2·s)[43,44]. Moreover, the present GCs are superior to rare-earth doped glasses in terms of the availability of a broad tuning range of wavelength. A comparison of the luminescent properties (λ_{peak}, peak emission wavelength, τ_{298K}, decay lifetime at the room temperature, and FOM) and crystal field parameters (Dq and B) of Ni^{2+} in GCs containing different spinels is shown in Table 1. The magnitude of crystal field strength Dq is a measure of the interaction of the 3*d*-electrons with the rest of the lattice, and the main contribution arises from the nearest neighbors. Although Ni^{2+} substitutes for Ga^{3+} in both ZGO and ZGGO GCs, the Dq value of the latter is slightly less than that of the former GCs, which, according to the ligand field theory, is due to the distortion of ligands inducing a weakening effect on the crystal field strength of the central ion[45].

It is important to stress that the synthesized $ZnGa_2O_4$: Ni^{2+} GCs are highly reproducible to allow for a fluctuation in the thermal treatment temperature, for example, transparent GCs with the broadband near NIR emission can be obtained at a crystallization temperature ranging from 750 to 800 °C (Fig. S9 in the supporting information). This is a very important advantage for the "melt-in-tube" method, for which the core fiber is covered with the SiO_2 cladding, and the heat transfer process during the heat treatment can be different from that of the glass sample. Because of different thermal treatment temperature, higher for the "melt-in-tube" method, GCs with required luminescent properties and transparency should be obtained in a temperature range as broad as possible.

In this respect, the studied ZGO GCs are perfectly matched to the "melt-in-tube" method, which will be the subject of our next study to succeed in making them into fibers.

Conclusion

The selective doping of Ni^{2+} in $ZnGa_2O_4$ and $Zn_{1+x}Ga_{2-2x}Ge_xO_4$ nano-spinels via the controlled crystallization results in a broadband NIR emission. The use of nucleating agents such as TiO_2 promotes occupation of the octahedral Ga^{3+} sites by Ni^{2+} and leads to enhanced luminescence and prolonged lifetime, whereas the partition of Ge^{4+} in $ZnGa_2O_4$ spinels leads to a reduced NIR emission, which is assumed to be related to the formation of anti-site defects. The large mismatch of valence and ionic radii between $^6Ni^{2+}$ and $^6Ge^{4+}$ considerably limits the substitution of $^6Ni^{2+}$ for $^6Ge^{4+}$, which also partly accounts for the comparatively weaker NIR emission from the $Zn_{1+x}Ga_{2-2x}Ge_xO_4$: Ni^{2+} GCs. The stronger NIR emission, excellent optical quality and reproducibility, as well as a tolerance for thermal treatment temperature make $ZnGa_2O_4$: Ni^{2+} nano-spinels embedded GCs highly promising candidates for broadband fiber amplifiers. Future work will focus on fabricating GC fibers by the "melt-in-tube" method.

References

1. Gmachl, C. *et al*. Ultra-broadband semiconductor laser. *Nature* **415**, 883–887, doi:10.1038/415883a (2002).
2. Lin, C. G. *et al*. Broadband near-IR emission from cubic perovskite $KZnF_3$:Ni^{2+} nanocrystals embedded glass-ceramics. *Opt. Lett.* **40**, 5263–5266, doi:10.1364/OL.40.005263 (2015).
3. Hughes, M., Rutt, H., Hewak, D. & Curry, R. J. Spectroscopy of vanadium (III) doped gallium lanthanum sulphide chalcogenide glass. *Appl. Phys. Lett.* **90**, 031108, doi:10.1063/1.2432280 (2007).
4. Ren, J. *et al*. Broadband near-infrared emission of chromium-doped sulfide glass-ceramics containing Ga_2S_3 nanocrystals. *Opt. Lett.* **37**, 5043–5045, doi:10.1364/OL.37.005043 (2012).
5. Zhou, S. F. *et al*. Ligand-driven wavelength-tunable and ultra-broadband infrared luminescence in single-ion-doped transparent hybrid materials. *Adv. Funct. Mater.* **19**, 2081–2088, doi:10.1002/adfm.v19:13 (2009).
6. Zhou, S. F. *et al*. Simultaneous tailoring of phase evolution and dopant distribution in the glassy phase for controllable luminescence. *J. Am. Chem. Soc.* **132**, 17945–17952, doi:10.1021/ja108512g (2010).
7. Sigaev, V. N. *et al*. Nickel-assisted growth and selective doping of spinel-like gallium oxide nanocrystals in germano-silicate glasses for infrared broadband light emission. *Nanotechnology* **23**, 015708, doi:10.1088/0957-4484/23/1/015708 (2012).
8. Galoisy, L. *et al*. Overview of the environment of Ni in oxide glasses in relation to the glass colouration. *Phys. Chem. Glasses.* **46**, 394–399 (2005).
9. Shigemura, H. *et al*. Optical property and local environment of Ni^{2+} in fluoride glasses. *J. Phys. Chem. B* **102**, 1920–1925, doi:10.1021/jp973311d (1998).
10. Tkomatsu, A. Design and control of crystallization in oxide glasses. *J. Non-Cryst. Solids.* **428**, 156–175, doi:10.1016/j.jnoncrysol.2015.08.017 (2015).
11. Wu, B. T. *et al*. Energy transfer between Cr^{3+} and Ni^{2+} in transparent silicate glass ceramics containing Cr^{3+}/Ni^{2+} co-doped $ZnAl_2O_4$ nanocrystals. *Opt. Express* **16**, 2508–2513, doi:10.1364/OE.16.002508 (2008).
12. Suzuki, T., Murugan, G. S. & Ohishi, Y. Optical properties of transparent Li_2O-Ga_2O_3-SiO_2 glass-ceramics embedding Ni-doped nanocrystals. *Appl. Phys. Lett.* **86**, 131903, doi:10.1063/1.1891272 (2005).
13. Chen, D. Q., Wan, Z. Y., Zhou, Y. & Ji, Z. G. Cr^{3+}-doped gallium-based transparent bulk glass ceramics for optical temperature sensing. *J. Euro. Ceram. Soc.* **35**, 4211–4216, doi:10.1016/j.jeurceramsoc.2015.08.005 (2015).
14. Wu, B. T. *et al*. Enhanced broadband near-infrared luminescence from transparent Yb^{3+}/Ni^{2+} codoped silicate glass ceramics. *Opt. Express* **16**, 1879–1884, doi:10.1364/OE.16.001879 (2008).
15. Sigaev, V. N. *et al*. Light-emitting Ga-oxide nanocrystals in glass: a new paradigm for low-cost and robust UV-to-visible solar-blind converters and UV emitters. *Nanoscale* **6**, 1763–1774, doi:10.1039/c3nr05210a (2014).
16. Fang, Z. J. *et al*. Ni^{2+} doped glass ceramic fiber fabricated by melt-in-tube method and successive heat treatment. *Opt. Express* **23**, 28258–28263, doi:10.1364/OE.23.028258 (2015).
17. Lin, C. G. *et al*. Oxyfluoride glass-ceramics for transition metal ion based photonics: broadband Near-IR luminescence of nickel ion dopant and nanocrystallization mechanism. *J. Phys. Chem. C.* **120**, 4556–4563, doi:10.1021/acs.jpcc.6b00683 (2016).
18. Pan, Z., Lu, Y. Y. & Liu, F. Sunlight-activated long-persistent luminescence in the near-infrared from Cr^{3+}-doped zinc gallogermanates. *Nat. Mater.* **11**, 58–63, doi:10.1038/nmat3173 (2011).
19. Ren, J. *et al*. Novel self-activated zinc gallogermanate phosphor: The origin of its photoluminescence. *J. Am. Ceram. Soc.* **97**, 3197–3201, doi:10.1111/jace.13103 (2014).
20. Abdukayum, A., Chen, J. T., Zhao, Q. & Yan, X. P. Functional near infrared-emitting Cr^{3+}/Pr^{3+}co-doped zinc gallogermanate persistent luminescent nanoparticles with superlong afterglow for *in vivo* targeted bioimaging. *J. Am. Chem. Soc.* **135**, 14125–14133, doi:10.1021/ja404243v (2013).
21. Zhuang, Y. X., Ueda, J. & Tanabe, S. Multi-color persistent luminescence in transparent glass ceramics containing spinel nanocrystals with Mn^{2+} ions. *Appl. Phys. Lett.* **105**, 191904-1–191904-4, doi:10.1063/1.4901749 (2014).
22. Chenu, S. *et al*. Tuneable nanostructuring of highly transparent zinc gallogermanate glasses and glass-ceramics. *Adv. Opt. Mater.* **2**, 364–372, doi:10.1002/adom.v2.4 (2014).
23. Chenu, S. *et al*. Long-lasting luminescent $ZnGa_2O_4$:Cr^{3+} transparent glass-ceramics. *J. Mater. Chem. C.* **2**, 10002–10010, doi:10.1039/C4TC02081B (2014).
24. Fang, Z. J. *et al*. Bismuth-Doped Multicomponent Optical Fiber Fabricated by Melt-in-Tube Method. *J. Am. Ceram. Soc.* **99**, 856–859, doi:10.1111/jace.2016.99.issue-3 (2016).
25. Fang, Z. J. *et al*. Fabrication and Characterization of Glass-Ceramic Fiber-Containing Cr^{3+} -Doped $ZnAl_2O_4$ Nanocrystals. *J. Am. Ceram. Soc.* **98**, 2772–2775, doi:10.1111/jace.2015.98.issue-9 (2015).
26. Dong, G. *et al*. Quantum dot-doped glasses and fibers: fabrication and optical properties. *Front. Mater.* 2, Article No. 13 (2015).
27. Yu, Y. Z. *et al*. Mesoscale engineering of photonic glass for tunable luminescence. *NPG Asia Materials* **8**, e318, doi:10.1038/am.2016.156 (2016).
28. Tanaka, K., Yamaguchi, I., Hirao, K. & Soga, N. Optical properties of transparent glass-ceramics containing $ZnGa_2O_4$: Cr^{3+}microcrystals. *Bull. Inst. Chem. Res., Kyoto Univ.* **72**, 124–133 (1994).
29. Takahashi, Y. *et al*. Defect activation in willemite-type Zn_2GeO_4 by nanocrystallization. *Appl. Phys. Lett.* **97**, 071906, doi:10.1063/1.3481081 (2010).
30. Loiko, P. A. *et al*. Influence of NiO on phase transformations and optical properties of ZnO-Al_2O_3-SiO_2 glass-ceramics nucleated by TiO_2 and ZrO_2. Part II. Optical absorption and luminescence. *J Non-Cryst Solids* **376**, 99–105, doi:10.1016/j.jnoncrysol.2013.05.031 (2013).
31. Suzuki, T., Horibuchi, K. & Ohishi, Y. Structural and optical properties of ZnO-Al_2O_3-SiO_2 system glass-ceramics containing Ni^{2+}-doped nanocrystals. *J. Non-Cryst. Solids* **255**, 2304–2309, doi:10.1016/j.jnoncrysol.2005.06.015 (2005).

32. Pinckney, L. R. Transparent, high strain point spinel glass-ceramics. *J. Non-Cryst. Solids* **255**, 171–177, doi:10.1016/S0022-3093(99)00368-3 (1999).
33. Dugué, A. *et al.* Structural evolution of Ni environment in lithium, magnesium and zinc aluminosilicate glasses and glass-ceramics. *J. Non-Cryst. Solids* **413**, 24–33, doi:10.1016/j.jnoncrysol.2015.01.011 (2015).
34. Cochain, B. *et al. In situ* local environment and partitioning of Ni^{2+} ions during crystallization of an oxyfluoride glass. *J. Non-Cryst. Solids* **408**, 7–12, doi:10.1016/j.jnoncrysol.2014.09.051 (2015).
35. Erwin, S. C. *et al.* Doping semiconductor nanocrystals. *Nature* **436**, 91–94, doi:10.1038/nature03832 (2005).
36. Brunold, T. C., Gudel, H. U. & Cavalli, E. Optical spectroscopy of Ni^{2+} doped crystals of Zn_2SiO_4. *Chem. Phys. Lett.* **268**, 413–420, doi:10.1016/S0009-2614(97)00237-6 (1997).
37. Allix, M. *et al.* Considerable improvement of long-persistent luminescence in germanium and tin substituted $ZnGa_2O_4$. *Chem. Mater.* **25**, 1600–1606, doi:10.1021/cm304101n (2013).
38. Xu, X. *et al.* Broadly tunable emission from Mn-doped zinc gallogermanate phosphors through composition modification. *Opt. Mater. Express* **4**(11), 2437–2440 (2014).
39. Gao, G. J., Peng, M. Y. & Wondraczek, L. Temperature dependence and quantum efficiency of ultrabroad NIR photoluminescence from Ni^{2+} centers in nanocrystalline Ba-Al titanate glass ceramics. *Opt. Lett.* **37**, 1166–1168, doi:10.1364/OL.37.001166 (2012).
40. Suzuki, T. & Ohishi, Y. Broadband 1400 nm emission from Ni^{2+} in zinc-alumino-silicate glass. *Appl. Phys. Lett.* **84**, 3804–3806, doi:10.1063/1.1741027 (2004).
41. Suzuki, T., Arai, Y. & Ohishi, Y. Quantum efficiencies of near-infrared emission from Ni^{2+}-doped glass-ceramics. *J. Lumin.* **128**, 603–609, doi:10.1016/j.jlumin.2007.10.010 (2008).
42. Wei, K. *et al.* Pr^{3+}-doped Ge-Ga-S glasses for 1.3 μm optical fiber amplifiers. *J. Non-Crystal. Solids* **182**, 257–261, doi:10.1016/0022-3093(94)00513-3 (1995).
43. Wei, K. *et al.* Spectroscopy of Dy^{3+} in Ge-Ga-S Glass and its Suitability for 1.3-μm Fiber-Optical Amplifier Applications. *Opt. Lett.* **19**, 904–906, doi:10.1364/OL.19.000904 (1994).
44. Ren, J. *et al.* Refractive index profile and luminescence properties of Dy^{3+}-doped $Ge_{20}Ga_5Sb_{10}S_{65}$ glass after electric field assisted silver diffusion. *J. Am. Ceram. Soc.* **94**(7), 1982–1985, doi:10.1111/jace.v94.7 (2011).
45. Zhou, S. *et al.* Intense Infrared Luminescence in Transparent Glass-Ceramics Containing β-Ga_2O_3:Ni^{2+}Nanocrystals. *J. Phys. Chem. C* **111**, 7335–7338, doi:10.1021/jp068370i (2007).

Acknowledgements

This study was supported by the National Natural Science Foundation of China (61227013, 51302082, 61307104, 61422505, 61405044 and 61575050), National Key Scientific Instrument and Equipment Development Project (No. 2013YQ040815), Program for New Century Excellent Talents in University (NCET-12-0623), Open Project Program of the Jiangsu Key Laboratory of Advanced Laser Materials and Devices (KLALMD-2015-07), the Fundamental Research Funds for the Central Universities and the 111 project (B13015) to the Harbin Engineering University.

Author Contributions

Z. Gao and J. Ren designed the experiments and wrote the draft. Y. Liu, X. Lu and Z. Fang did the measurements. E. Lewis, G. Farrell, J. Yang and P. Wang discussed the results and commented on the manuscript. All authors reviewed the manuscript.

Additional Information

Supplementary information accompanies this paper at doi:10.1038/s41598-017-01676-6

Competing Interests: The authors declare that they have no competing interests.

Publisher's note: Springer Nature remains neutral with regard to jurisdictional claims in published maps and institutional affiliations.

Open Access This article is licensed under a Creative Commons Attribution 4.0 International License, which permits use, sharing, adaptation, distribution and reproduction in any medium or format, as long as you give appropriate credit to the original author(s) and the source, provide a link to the Creative Commons license, and indicate if changes were made. The images or other third party material in this article are included in the article's Creative Commons license, unless indicated otherwise in a credit line to the material. If material is not included in the article's Creative Commons license and your intended use is not permitted by statutory regulation or exceeds the permitted use, you will need to obtain permission directly from the copyright holder. To view a copy of this license, visit http://creativecommons.org/licenses/by/4.0/.

© The Author(s) 2017